Direct Speed Control based on Finite Control Set Model Predictive Control with Voltage Smoother

Hiroaki Kawai, *Member, IEEE*, Zhenbin Zhang, *Senior Member, IEEE*
Ralph Kennel, *Senior Member, IEEE,* and Shinji Doki, *Member, IEEE*

***Abstract*— A direct speed control strategy based on finite control set model predictive control (FCS–MPC) with a voltage smoother is presented herein. In the proposed concept, a finite set of smoothed voltage vectors characterized by an adjustable amplitude and a movable origin is introduced as voltage candidates in the FCS–MPC scheme. The controller predicts the future current and speed and outputs the optimal smoothed voltage using pulse-width modulation. Owing to this control scheme, an abrupt change in the output voltage, which causes a large current ripple, is avoided without additional computational costs. Simulation and experimental results obtained using a permanent magnet synchronous motor fed by a two-level three-phase inverter show that the proposed method effectively reduces the current ripple while achieving a high dynamic drive compared with the conventional FCS–MPC scheme.**

***Index Terms*— Direct speed control, finite control set model predictive control (FCS–MPC), permanent magnet synchronous motor (PMSM), pulse-width modulation (PWM), voltage smoother.**

I. Introduction

The speed control of electrical machines is vital to electric drive systems, and various techniques for implementing speed control have been investigated in the past decades. Field-oriented control with a proportional integral (PI) cascaded structure, which can yield a stable drive performance by setting the appropriate gain parameters, is typically used in speed control applications [1]–[3]. However, the bandwidth of the controller cannot be expanded to the high-frequency side beyond a certain level while avoiding overshoots, undershoots, and oscillations. Furthermore, the bandwidth of the outer-loop speed controller should be set smaller than that of the inner loop current controller. Therefore, improvements in the dynamic performance of electric drives are limited if the control algorithm is based on this strategy.

Among the advanced techniques whose concepts differ from those of the feedback-based classical approach, predictive control has been investigated extensively in the fields of power electronics and electrical drives [4]. In the classification of this method, model predictive control (MPC) [5], which primarily comprises a continuous control set MPC [6]–[8] and a finite control set MPC (FCS–MPC) [9]–[12], is one of the most active research areas in recent years. MPC offers a high dynamic performance and can manage the nonlinearities of a plant and constraints such as the current limit or voltage limit. Furthermore, powerful microprocessors, which can execute the MPC algorithm during the short sampling time required for power electronics control, have recently become available. Hence, it has been widely introduced as a control strategy for electric machines such as induction motors [13]–[15] and permanent magnet synchronous motors (PMSMs) [16]–[20]. Although these studies are aimed at current or torque control, MPC schemes can be expanded to speed control without a cascaded structure.

A direct speed control scheme based on FCS–MPC was investigated to overcome the limit of the dynamic performance [21]–[23]. As the future states of an electric motor, (i.e., both current and speed) are directly predicted in discrete steps using a finite set of voltage vectors, a cascade structure is not required in these control schemes. Simulation and experimental results from previous studies showed superior tracking performance with respect to the reference speed; however, current ripples occurred, particularly in the steady-state operation. In FCS–MPC, the controller outputs the voltage, which is selected from the finite set of voltage vectors at each sampling time; therefore, the output voltage will change abruptly [24]. Moreover, in simulations and practical implementations of FCS–MPC, the real switching frequency tends to be lower than its theoretical maximum value [25]. Therefore, a current ripple with a large amplitude, which can cause torque ripples, mechanical vibrations, noise, and losses, is generated. The suppression of current ripples in FCS–MPC is a technical problem that must be solved to enable its industrial use. A faster sampling period is

Manuscript received March 24, 2022; accepted April 25, 2022.

H. Kawai is with Applied Physics Research Laboratory, Technical Development Group, Kobe Steel, Ltd., Kobe, 651-2271, Japan, and also with the Department of Information and Communication Engineering, Nagoya University, Nagoya, 461-0861, Japan (e-mail: kawai.hiroa-ki@kobelco.com; kawai.hiroaki@nagoya-u.jp)

Z. Zhang is with the School of Electrical Engineering, Shandong University, Jinan, 250061, China (e-mail: zbz@sdu.edu.cn)

R. Kennel is with the chair of Electrical Drive Systems and Power Electronics, Munich, 80333, Germany (e-mail: ralph.kennel@tum.de).

S. Doki is with the Department of Information and Communication Engineering, Nagoya University, Nagoya, 464-8601, Japan (e-mail: doki@nagoya-u.jp)

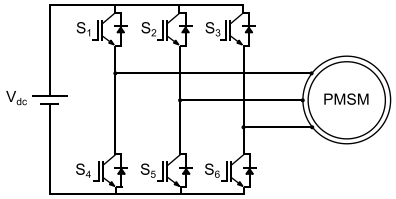

Fig. 1. PMSM drive system.

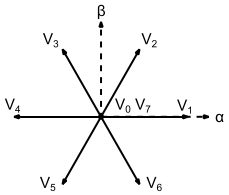

Fig. 2. Voltage vectors yielded by two-level three-phase inverter.

efficient for reducing current ripples. However, the computing power of the micro-control unit is limited and cannot be reduced significantly.

Several strategies have been investigated to overcome this drawback [25]–[28]. In [25] and [26], a variable switching point was presented to minimize torque ripples. The experimental results showed favorable performance under steady-state and transient operating conditions. However, improvements in current and torque ripple reduction were limited, and the computational effort increased owing to additional calculations for future state prediction at the present variable switching point. In [27], a control scheme that switched modulation-based PI control and FCS–MPC based on the driving situation was proposed. The simulation results showed favorable performance in terms of current ripple reduction during steady-state operation. However, the control algorithm was complicated because two completely different control methods were required. Moreover, it was difficult to switch the two algorithms without incurring a discontinuous change in the output torque and speed. In [28], a suitable search space for determining the optimum output voltage in the FCS–MPC scheme was introduced. The experimental results showed excellent performance for current ripple suppression compared with the traditional approach. However, the computational cost will increase significantly because of the increased size of the search space.

Modulation-based MPC, CCS-MPC [6]–[8] is expected to maintain a low current ripple owing to its continuous output voltage. However, this strategy has a complex formulation to solve the optimization problem and requires considerable effort to achieve controller implementation.

A deadbeat control with modulator [29], [30] is effective strategy to achieve fast transient response. However, the controller cannot handle the control constraints [4]. In addition, the control performance is sensitive to parameter mismatch in the model, and the remarkable steady-state error occurs without any compensation in simple current control [31]. This low robustness can be a problem to achieve speed control based on deadbeat-based strategy.

Herein, direct speed control based on FCS–MPC with a voltage smoother is presented, where voltage candidates in the FCS–MPC scheme are created using a smoothing concept initially introduced in [24]. In this method, a finite set of smoothed voltage vectors with adjustable magnitudes is arranged around the previous output voltage as voltage candidates. The controller selects the optimal smoothed voltage vector through the prediction process and applies it using an inverter with a pulse-width modulator. Based on the proposed strategy, an abrupt change in the output voltage, which yields a current ripple with a large amplitude, can be avoided without high additional computational costs. In addition, an arbitrary magnitude voltage can be output; however, the algorithm is based on FCS–MPC. Therefore, the advantages of FCS–MPC in addition to those previously discussed, such as less complex formulation, can be inherited while improving the previously described drawback. The strategy for the proposed direct speed control for PMSMs involving the smoothing concept is presented comprehensively herein, and the simulation and experimental results for assessing the performance of the proposed method including additional results are compared with the results from [24].

II. Finite Control Set Model Predictive Control

A PMSM and a two-level three-phase voltage source inverter were emphasized in this study, as shown in Fig. 1. In this section, the numerical models of the PMSM drive systems and the principles of FCS–MPC for speed control are summarized.

A. PMSM model

The continuous model of the PMSM in the dq frame is described as follows:

$$\dot{i}_d = -\frac{R}{L_d} i_d + \frac{L_q}{L_d} \omega_e i_q + \frac{1}{L_d} v_d \tag{1}$$

$$\dot{i}_q = -\frac{R}{L_q} i_q - \frac{L_d}{L_q} \omega_e i_d - \frac{\psi}{L_q} \omega_e + \frac{1}{L_q} v_q \tag{2}$$

R represents the stator resistance, and ψ the flux linkage of the permanent magnet. L_d and L_q denote the d- and q-axis inductances, respectively, and ω_e the electrical rotor speed. Meanwhile, i_d and i_q denote the d- and q-axis currents, respectively; v_d and v_q denote the d- and q-axis voltages, respectively.

The electric torque T_e is calculated using the following equation, where p represents the number of pole pairs:

$$T_e = \frac{3}{2} p(\psi i_q + (L_d - L_q) i_d i_q) \tag{3}$$

The mechanical model of the PMSM involving a load torque is expressed as

$$\dot{\omega}_m = -\frac{D}{J} \omega_m + \frac{1}{J}(T_e - T_l), \tag{4}$$

where D is the mechanical friction coefficient, J the rotor inertia, T_l the load torque, and $\omega_m = \omega_e / p$ the mechanical rotor speed.

The continuous models expressed in (1), (2), (3), and (4) are discretized with the sampling time T_s as follows:

$$i_d(k+1) = \left(1 - \frac{T_s R}{L_d}\right) i_d(k) + \frac{T_s L_q}{L_d} \omega_e(k) i_q(k) + \frac{T_s}{L_d} v_d(k) \tag{5}$$

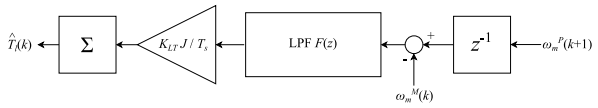

Fig. 3. Structure of load torque observer [34].

$$i_q(k+1)=\left(1-\frac{T_sR}{L_q}\right)i_q(k)-\frac{T_sL_d}{L_q}\omega_e(k)i_d(k)-\frac{T_s\psi}{L_q}\omega_e(k)+\frac{T_s}{L_q}v_q(k) \tag{6}$$

$$T_e(k+1)=\frac{3}{2}p(\psi+(L_d-L_q)i_d(k+1))i_q(k+1) \tag{7}$$

$$\omega_m(k+1)=\frac{J-T_sD}{J}\omega_m(k)+\frac{T_s}{J}(T_e(k)-T_l(k)). \tag{8}$$

The results presented herein were obtained using a surface-mounted permanent magnet synchronous motor (SPMSM). Hence, the d- and q-axis inductances in the previous numerical model were equal, i.e.,

$$L_d=L_q=L. \tag{9}$$

B. Inverter model

A two-level three-phase inverter, which comprises six switching power devices, can yield voltage vectors, as shown in Fig. 2. The relationships between the inverter output voltage and switching states are described as follows:

$$S_a=\begin{cases}1, & S_1:\text{on}\quad S_4:\text{off}\\ 0, & S_1:\text{off}\quad S_4:\text{on}\end{cases} \tag{10}$$

$$S_b=\begin{cases}1, & S_2:\text{on}\quad S_5:\text{off}\\ 0, & S_2:\text{off}\quad S_5:\text{on}\end{cases} \tag{11}$$

$$S_c=\begin{cases}1, & S_3:\text{on}\quad S_6:\text{off}\\ 0, & S_3:\text{off}\quad S_6:\text{on}\end{cases} \tag{12}$$

$$\mathbf{S}=\frac{2}{3}(S_a+e^{j\frac{2}{3}\pi}S_b+e^{j\frac{4}{3}\pi}S_c) \tag{13}$$

$$\mathbf{V}=V_{dc}\mathbf{S} \tag{14}$$

In the equation above, V is the output voltage vector, and V_{dc} is the DC link voltage.

C. Control Strategy

The primary control scheme of this work is based on direct speed control [20], which is an expanded predictive current control technique [10]. In this strategy, the voltage vector is selected as the optimal control output among a finite set of voltage vectors through evaluation using a cost function. Hence, the cost function is an important element as it determines the control performance. In this study, the evaluation value was determined using three terms: speed error, current error, and control constraints [20]. For speed control, the minimization of the error between the reference and measured rotor speeds is the primary goal. In the SPMSM, i_d should be minimized such that the input energy is minimized as well. Furthermore, the controller must regulate the current within the limitations stipulated in the drive system specifications. Therefore, the cost function was designed as follows:

$$g=a\sum_{i=1}^{N_p}g_S(k+i)+b\sum_{i=1}^{N_p}g_C(k+i)+c\sum_{i=1}^{N_p}g_L(k+i) \tag{15}$$

$$g_S(k)=\left(\omega_m^*(k)-\omega_m(k)\right)^2 \tag{16}$$

$$g_C(k)=\left(0.0-i_d(k)\right)^2 \tag{17}$$

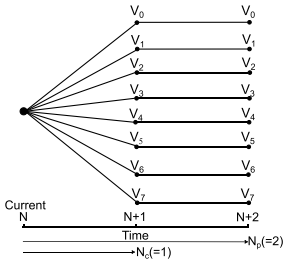

Fig. 4. Possible voltage vectors with N_p = 2 and N_c = 1.

$$g_L(k)=\begin{cases}I_E(k)^2 & (I_E(k)<0)\\ 0 & (I_E(k)\geq 0)\end{cases} \tag{18}$$

$$I_E(k)=I_L-\sqrt{i_d(k)^2+i_q(k)^2} \tag{19}$$

Here, a, b, and c are the weighting factors, whereas I_L is the limiting value of the winding current of the electric motor. Note that the reference current in the d-axis is set to zero, that is, the weakening flux region is not the focus of this study.

For direct speed control, a load torque is necessitated to predict the future speed using (8); however, the use of the sensor is restricted owing to its volume, weight, cost, and reliability. Therefore, a load torque estimation technique using an observer was adopted in this study. Although several strategies for load torque estimation have been proposed [32], [33], state observer-based prediction error correction [34] was applied in this study because of its simple structure and low computational power. The estimated load torque $\hat{T}_l$ was calculated by the observer as follows:

$$\hat{T}_l(k)=\hat{T}_l(k-1)+K_{LT}\frac{J}{T_s}\left(\omega_m{}^P(k)-\omega_m{}^M(k)\right) \tag{20}$$

Here, $\omega_m{}^P$ is the predicted speed at the previous time step in the FCS–MPC scheme, $\omega_m{}^M$ is the measured speed, and K_{LT} is the gain parameter. The tuning result of the gain parameter K_{LT} significantly affects the tracking performance to the reference speed and must be tuned to satisfy both the control stability and responsiveness of speed control. Hence, as summarized following, the value of K_{LT} was determined based on the tuning method described in [34].

The prediction speed error resulting from using the observer integrated with LPF for reducing encoder signal noise depicted in Fig. 3 can be expressed as followings.

$$\Delta\omega=\omega_m{}^P-\omega_m{}^M \tag{21}$$

$$\Delta\omega=\frac{T_s}{J}z^{-1}T_l-K_{LT}\frac{z^{-1}}{1-z^{-1}}F(z)\Delta\omega \tag{22}$$

$$F(z)=\frac{b_0+b_1z^{-1}+b_2z^{-2}}{a_0+a_1z^{-1}+a_2z^{-2}} \tag{23}$$

Therefore, the transfer function between the load torque as input and the prediction error as output is derived as follow.

$$H(z)=\frac{\Delta\omega}{T_l} \tag{24}$$
$$=\frac{a_0T_sz^3+(a_1-a_0)T_sz^2+(a_2-a_1)T_sz-a_2T_s}{a_0Jz^4+(K_{LT}b_0+a_1-a_0)Jz^3+(K_{LT}b_1+a_2-a_1)Jz^2+(K_{LT}b_2-a_2)Jz}$$

To satisfy the stability of the prediction process, and thus the stability of direct speed control, the poles of $H(z)$ should be lied in the stabile region. In this study, the value of K_{LT} was set to 0.09 in accordance with the criteria listed in [34].

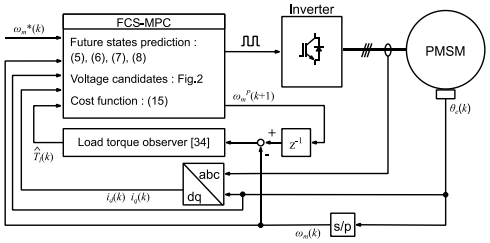

Fig. 5. Control block diagram of conventional FCS–MPC.

In this study, the predicted horizon N_p and control horizon N_c, which constitute the parameters in the FCS–MPC scheme, were set as 2 and 1, respectively. In this setting, the controller calculates the future current and speed for all possible voltage vectors, as shown in Fig. 4.

The different steps at every control sampling are described below, and the control block diagram of direct speed control based on FCS–MPC is shown in Fig. 5.

STEP1: Measure the machine currents $i_d(k)$ and $i_q(k)$, as well as the rotor speed $\omega_m(k)$.

STEP2: Predict the future states for the next sampling time $i_d(k+1)$, $i_q(k+1)$, and $\omega_m(k+1)$ using the discrete models expressed in (5), (6), (7), and (8) while estimating the load torque $\hat{T}_l(k)$ based on (20). This step is executed to compensate for the discrete delay caused by the computing process in a digital control system [35].

STEP3: Predict the future currents $[\boldsymbol{i}_{dq}(k+2), \boldsymbol{i}_{dq}(k+3)]$ and speed states $[\omega_m(k+2), \omega_m(k+3)]$ using the discrete models expressed in (5) to (8) and the load torque estimated in STEP2 for all possible voltage vectors.

STEP4: Determine the value of the cost function (15) for each voltage vector.

STEP5: Select the voltage vector with the smallest value in STEP4 as the best voltage vector. The controller yields a gate-drive signal corresponding to the optimal output voltage.

III. Finite Control Set Model Predictive Control with a Voltage Smoother

In FCS–MPC, the best voltage vector, which is selected from a finite set of voltage vectors through optimization, is assigned as the commanding voltage. Therefore, an abrupt change in the output voltage occurs, resulting in a large current ripple, as stated previously. To overcome this drawback, a finite set of smoothed voltage vectors is introduced in the proposed strategy as follows:

$$\boldsymbol{v}_{dqs}{}^{i}(k) = K_\alpha \boldsymbol{v}_{dqs}(k-1) + (1-K_\alpha)\boldsymbol{v}_{dq}{}^{i} \tag{25}$$

$$\mathbf{v}_{dq}{}^{i}(k) = \mathbf{PV}_i \tag{26}$$

$$\mathbf{P} = \begin{bmatrix} \cos\theta_e & \sin\theta_e \\ -\sin\theta_e & \cos\theta_e \end{bmatrix} \tag{27}$$

The quantity $\boldsymbol{v}_{dqs}{}^{i} = [v_{ds}{}^{i}, v_{qs}{}^{i}]^{\mathrm{T}}$ is the dq-axis smoothed voltage, and $\boldsymbol{v}_{dq}{}^{i} = [v_d{}^{i}, v_q{}^{i}]^{\mathrm{T}}$ represents the dq-axis voltage transformed into the dq-plane of the voltage vectors depicted in Fig. 2 using Park's transformation (26) and (27). The integer i corresponds to the vector numbers shown in Fig. 2. The parameter K_α is in the interval [0, 1) and allows for the adjustment of the voltage smoothness, that is, the larger the K_α, the more prominent is the smoothness. The smoothed voltages at a certain time step are obtained from those at the previous time step and the dq-axis voltage $\boldsymbol{v}_{dq}{}^{i}$ based on (25), where the parameters are listed in Table I. The future current and speed are predicted using the smoothed voltage $\boldsymbol{v}_{dqs}{}^{i}$ as the input voltage for the PMSM model. Hence, the numerical models for future current predictions (5) and (6) are rewritten as follows:

TABLE I
Parameters for Calculating Smoothed Voltages

i	$\mathbf{v}_{dqs}{}^{i}(N+1)$		$\mathbf{v}_{dqs}{}^{i}(N+2)$	
	$\mathbf{v}_{dqs}(k\text{-}1)$	$\mathbf{v}_{dq}{}^{i}$	$\mathbf{v}_{dqs}(k\text{-}1)$	$\mathbf{v}_{dq}{}^{i}$
0	Output voltage at step N.	$\mathbf{v}_{dq}{}^{0}(=\mathbf{PV}_0)$	$\mathbf{v}_{dqs}{}^{0}(N+1)$	$\mathbf{v}_{dq}{}^{0}(=\mathbf{PV}_0)$
1		$\mathbf{v}_{dq}{}^{1}(=\mathbf{PV}_1)$	$\mathbf{v}_{dqs}{}^{1}(N+1)$	$\mathbf{v}_{dq}{}^{1}(=\mathbf{PV}_1)$
2		$\mathbf{v}_{dq}{}^{2}(=\mathbf{PV}_2)$	$\mathbf{v}_{dqs}{}^{2}(N+1)$	$\mathbf{v}_{dq}{}^{2}(=\mathbf{PV}_2)$
3		$\mathbf{v}_{dq}{}^{3}(=\mathbf{PV}_3)$	$\mathbf{v}_{dqs}{}^{3}(N+1)$	$\mathbf{v}_{dq}{}^{3}(=\mathbf{PV}_3)$
4		$\mathbf{v}_{dq}{}^{4}(=\mathbf{PV}_4)$	$\mathbf{v}_{dqs}{}^{4}(N+1)$	$\mathbf{v}_{dq}{}^{4}(=\mathbf{PV}_4)$
5		$\mathbf{v}_{dq}{}^{5}(=\mathbf{PV}_5)$	$\mathbf{v}_{dqs}{}^{5}(N+1)$	$\mathbf{v}_{dq}{}^{5}(=\mathbf{PV}_5)$
6		$\mathbf{v}_{dq}{}^{6}(=\mathbf{PV}_6)$	$\mathbf{v}_{dqs}{}^{6}(N+1)$	$\mathbf{v}_{dq}{}^{6}(=\mathbf{PV}_6)$
7		$\mathbf{v}_{dq}{}^{7}(=\mathbf{PV}_7)$	$\mathbf{v}_{dqs}{}^{7}(N+1)$	$\mathbf{v}_{dq}{}^{7}(=\mathbf{PV}_7)$

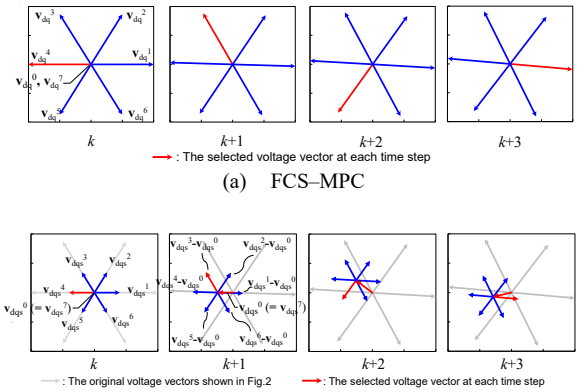

(a) FCS–MPC

(b) Proposed FCS–MPS with $K_\alpha = 0.6$

Fig. 6. Voltage candidates in dq-axis with ω_e = 3000 rpm and Ts = 100 μs.

$$i_d(k+1) = \left(1 - \frac{T_s R}{L_d}\right) i_d(k) + \frac{T_s L_q}{L_d}\omega_e(k) i_q(k) + \frac{T_s}{L_d} v_{ds}{}^{i}(k) \tag{28}$$

$$i_q(k+1) = \left(1 - \frac{T_s R}{L_q}\right) i_q(k) - \frac{T_s L_d}{L_q}\omega_e(k) i_d(k) - \frac{T_s \psi}{L_q}\omega_e(k) + \frac{T_s}{L_q} v_{qs}{}^{i}(k) \tag{29}$$

The output voltage candidates with the smoothing process are shown in Fig. 6, and they were compared with the traditional FCS–MPC approach. For simplicity, the electrical rotor speed ω_e was assumed to be constant at 3000 rpm. The voltage candidates, which were converted from those in the $\alpha\beta$-axis shown in Fig. 2, rotated in the dq-axis. As shown in Fig. 5, the proposed strategy reduced the amplitude while shifting the center of the voltage candidates within the operating range. Hence, abrupt changes in the output voltage were avoided. Incidentally, the smaller the K_α, the closer the output voltage candidates are to the conventional value, and this is exactly the same as before when K_α is set to zero.

According to (25), the smoothed voltage candidates are produced from the voltage vector $\boldsymbol{v}_{dq}{}^{i}$ by the low-pass filter (LPF) action. Here, a larger K_α may lead to an impaired response in the output voltage and control performance. In this study, this parameter was set such that the dynamic performance remained at the same level as that of the conventional method.

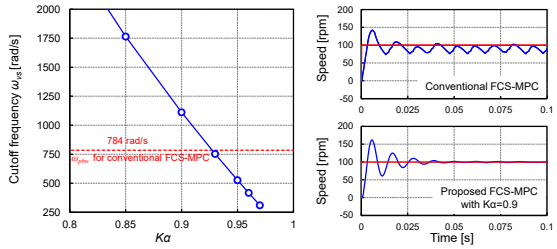

Fig. 7. Cutoff frequency of voltage smoothing process (left : relation between cutoff frequency and $K\alpha$, right : simulation results for step response) .

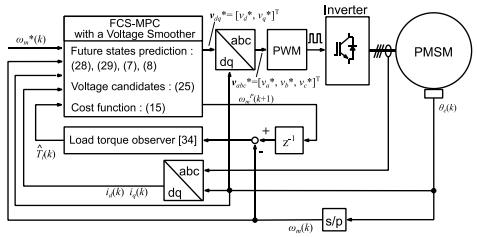

Fig. 8. Control block diagram of proposed FCS–MPC.

First, (25) can be regarded as a 1st order LPF discretized with sampling time T_s, and the cutoff frequency is expressed as follows:

$$\omega_{vs} = \frac{1-K_\alpha}{K_\alpha T_s} \tag{30}$$

The relationship between ω_{vs} and K_α was obtained, as shown in Fig. 7. Next, the conventional FCS–MPC bandwidth was obtained. In [20], the practical bandwidth based on the Gaussian response was introduced to assess the dynamic behavior of the FCS–MPC scheme and was obtained as follows:

$$\omega_{pbw} = 2\pi \frac{0.34}{t_r} \tag{31}$$

The parameter t_r is the step response rise time between 10 and 90%. In this study, the conventional FCS–MPC practical bandwidth was determined to be 784 rad/s from the simulation results shown in Fig. 7. Finally, parameter K_α is selected to satisfy $\omega_{vs} > \omega_{pbw}$. Therefore, it is expected that the control system bandwidth with the smoothing process (25) is maintained at the same level as that of the conventional strategy, and thus, the upper limit of K_α was set to 0.9. For reference purposes, the simulation result for the proposed FCS–MPC with $K_\alpha = 0.9$ is shown in Fig. 7.

The different steps pertaining to the proposed control scheme are described below, and the control block diagram of direct speed control based on FCS–MPC with voltage smoother is shown in Fig. 8. The PWM modulator is integrated with the control scheme to output the optimum smoothed voltage which is not identical to the voltage vectors shown in Fig. 2 and cannot be produced with a single switching state.

STEP1: Measure the machine currents $i_d(k)$ and $i_q(k)$, as well as the rotor speed $\omega_m(k)$.

STEP2: Predict the future states for the next sampling time $i_d(k+1)$, $i_q(k+1)$, and $\omega_m(k+1)$ using the discrete models expressed in (28), (29), (7), and (8) while estimating the load torque $\hat{T}_l(k)$ based on (20). This step is executed to compensate for the discrete delay caused by the computing process [35].

TABLE Ⅱ
PARAMETERS FOR PMSM DRIVE SYSTEM

Electrical Machine: SPMSM	
Stator resistance R	26.3 [Ω]
Inductance L	47.4 [mH]
PM flux linkage ψ	0.27 [Wb]
Pole pairs p	3
Inertia J (except for load machine)	$6.5\cdot10^{-5}$ [kg m^2]
Friction D	$1.0\cdot10^{-3}$ [kg m^2/s]
Power	210 [W]
Rated speed	2000 [rpm]
Rated torque	1.0 [N m]
Rated AC current	0.8 [A]
Inverter and controller	
DC link voltage Vdc	560 [V]
Sampling time Ts	100 [μs]
Carrier frequency f_c	10 / 8 / 6 / 3.5 [kHz]
Prediction and control horizon N_p / N_c	2 / 1
Weighting factors a / b / c	1.0 / 5.0 / 1000.0
Current limitation I_L	2.5 [A]

STEP3: Calculate the smoothed voltages (25) at the next two sampling instants [$\boldsymbol{v}_{dqs}{}^i(k+1)$, $\boldsymbol{v}_{dqs}{}^i(k+2)$] for all eight voltage vectors, as shown in Fig. 3.

STEP4: Predict the future currents [$\boldsymbol{i}_{dq}(k+2)$, $\boldsymbol{i}_{dq}(k+3)$], speed states [$\omega_m(k+2)$, $\omega_m(k+3)$] for all smoothed voltages derived in STEP3 using the discrete models expressed in (28), (29), (7), (8) and the load torque estimated in STEP2.

STEP5: Determine the value of the cost function (15) for each smoothed voltage vector.

STEP6: Select the smoothed voltage with the smallest value among $\boldsymbol{v}_{dqs}{}^i(k+1)$ as the best smoothed voltage $\boldsymbol{v}_{dq}{}^*$. Finally, the optimal voltage $\boldsymbol{v}_{dq}{}^*$ is transformed into the *abc* plane, $\boldsymbol{v}_{abc}{}^*$, and the PWM generator produces the gate drive signals while using $\boldsymbol{v}_{abc}{}^*$ as the reference voltage, as depicted in Fig. 8.

IV. EVALUATION

To investigate the performance, the proposed method was tested both numerically and experimentally. The characteristics of the drive system involving the PMSM are listed in Table II. In addition, for the quantitative performance assessment, the following criteria are introduced: (a) The overshoot for the reference speed $\Delta\omega_{m\,os}$, (b) the transient speed error after load torque application $\Delta\omega_{m\,LT}$, (c) the settling time for 2% tolerance band t_{st}, and (d) the standard deviation of the dq-axis current at the time between t_1 and t_2 $\sigma_{[t1,t2]}$.

A. Simulation results

The proposed direct speed control algorithm based on FCS–MPC with a voltage smoother was implemented in MATLAB/Simulink. To compare its performance, speed control based on the conventional FCS–MPC was evaluated under the same simulation conditions. In the simulation, the load machine inertia of $5.8\cdot10^{-4}$ kg m^2, which is unknown to the controller, was modeled to simulate under the same configuration as that used in the experiment.

Fig. 9 shows the simulation result of the proposed speed control using FCS–MPC with a voltage smoother. The PWM carrier frequency f_c was set to 10 kHz, which is equal to the control sampling, and the parameter K_α in (25) was set to 0.3, 0.6, and 0.9. The reference speed was increased from 0 to 1000 rpm with constant acceleration and maintained at 1000 rpm.

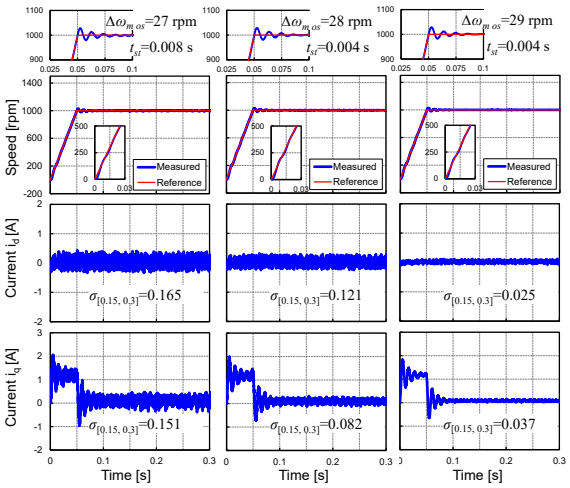

Fig. 9. Simulation results for speed-control-based proposed FCS–MPC with f_c = 10 kHz (left : K_α = 0.3, middle : K_α = 0.6, right : K_α = 0.9).

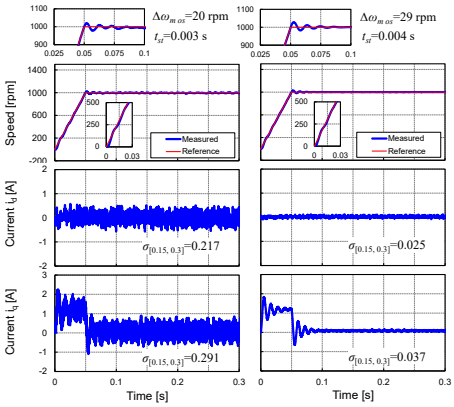

Fig. 10. Simulation results for the speed control: comparison with the conventional FCS–MPC (left: conventional FCS–MPC, right: proposed FCS–MPC with K_α = 0.9 and f_c = 10 kHz).

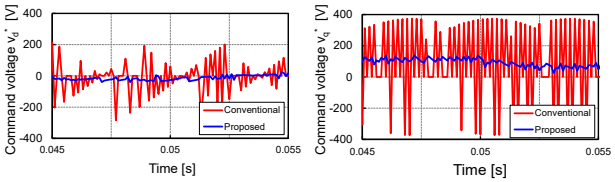

Fig. 11. Command voltage in d- and q-axes.

Load torque was not applied, except for the load machine inertia. As the value of K_α increased, the current ripples in the d- and q-axes reduced effectively. In addition, the speed tracking performance among the three parameter settings did not differ significantly.

Fig. 10 shows a performance comparison between the conventional and proposed FCS–MPC. In the proposed method, f_c and K_α were set to 10 kHz and 0.9, respectively. In the conventional FCS–MPC, the measured speed is the same as the reference speed with a fast response. However, a large ripple occurs in the d- and q-axis currents. Conversely, in the proposed method, the current ripple in the d- and q-axes was effectively reduced while fast dynamics was achieved in speed control. The overshoot and settling time were increased compared to those of the conventional method, although not significantly. In Fig. 11, the command voltage during the simulation shown in Fig. 10 is presented. For comparison, the optimum voltage vector selected in the conventional FCS–MPC scheme was transformed to the dq-axis and presented. In

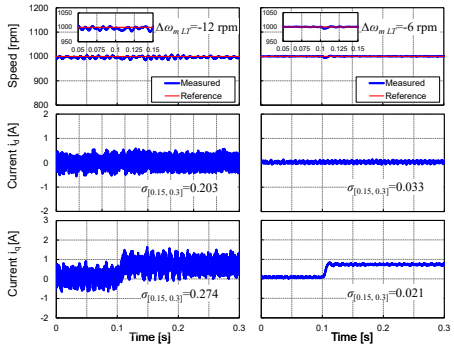

Fig. 12. Simulation results for speed control: comparison with conventional FCS–MPC under load torque change (left: conventional FCS–MPC; right: proposed FCS–MPC with K_α = 0.9 and f_c = 10 kHz).

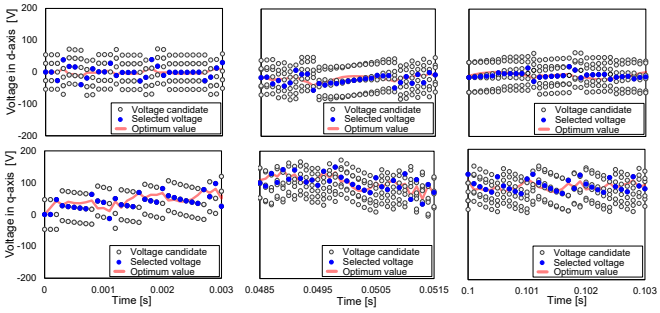

Fig. 13. Voltage candidates and selected voltages in proposed FCS–MPC with K_α = 0.9 (left: during acceleration in Fig.10; middle: during transition to constant speed in Fig.10; right: after applying load torque in Fig.12).

the proposed method, the variation in the command voltage between sampling times was suppressed significantly owing to the smoother voltage compared with the conventional FCS–MPC. Therefore, an abrupt change in the output voltage was avoided, and low current ripple was achieved.

Fig. 12 presents the simulation results of speed control under a load torque change. In the simulation, a load torque of 0.8 Nm was applied at 0.1 s. Similar to the simulation result shown in Fig. 10, the current ripple in the d- and q-axes reduced significantly when the proposed method was used. Moreover, the measured speed reflected the reference target even when a load torque change occurred. Moreover, the transient speed error was large compared to the proposed strategy; however, the deviation was caused by its original speed ripple as well as the load torque application.

Fig. 13 shows the smoothed voltage candidates produced by the equation (25) and the selected voltages v_{dq}^* in the proposed method. As a reference, the optimum solution, which is obtained through an exhaustive search with the resolution of 0.5 V, is depicted. The voltage candidates are generated to cover the location of the optimum solution, and the selected voltages v_{dq}^*, which is determined by a simple optimization procedure based on FCS-MPC, are consistent with the optimal value, except for a small quantization error.

Fig. 14 shows the simulation results for the performance comparison of parameter variations in the conventional FCS–MPC. In this simulation, to assess the performance when the calculation cost was increased, the parameter settings of the predicted horizon N_p, control horizon N_c, and sampling time T_s in the conventional FCS–MPC were replaced with the values listed in Table III. For the conventional FCS–MPC, the current ripple in the d- and q-axes can be reduced by reducing the

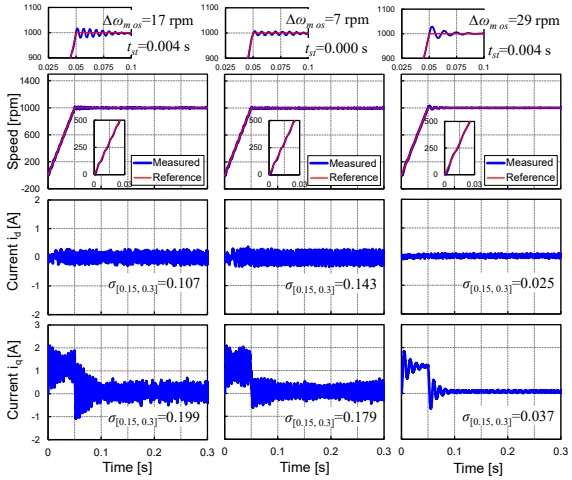

Fig. 14. Performance comparison of parameter variations in conventional FCS–MPC (left: FCS–MPC with $N_p = 2$, $N_c = 1$, and $T_s = 50$ μs; middle: FCS–MPC with $N_p = 3$, $N_c = 1$, and $T_s = 50$ μs; right: proposed FCS–MPC with $K_\alpha = 0.9$, $N_p = 2$, $N_c = 1$, $T_s = 100$ μs and $f_c = 10$ kHz).

TABLE Ⅲ
COMPARISON OF COMPUTATIONAL COSTS

Method	T_s / N_p / N_c	Computational cost per 100μs	
		Number of iterations	Execution time ratio
Conventional FCS–MPC	100 μs / 2 / 1	17	1.00
	50 μs / 2 / 1	34	2.07
	50 μs / 3 / 1	50	2.94
Proposed	100 μs / 2 / 1	17	1.06

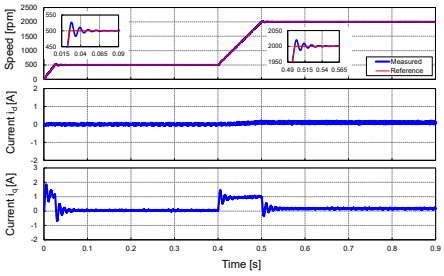

Fig. 15. Simulation results for speed control up to the rated speed with proposed FCS–MPC ($K_\alpha = 0.9$, $f_c = 10$ kHz).

sampling time and increasing the predicted horizon; however, the suppression level is limited. In addition, the execution time ratio, which is derived from the average run time when the C language function is called 5×10^5 times on an Intel Core i5 2.4 GHz dual core machine, are listed in Table III. According to the results, the computational burdens increased depending on the number of iterations to calculate the future states using the discrete models, as previously discussed. Conversely, in the proposed FCS–MPC, the current ripple can be effectively reduced while maintaining the execution time at the same level as the standard FCS–MPC with T_s=100μs and N_p=2. Based on these results, it can be inferred that the proposed method is effective for driving an electric motor with high dynamics while reducing the current ripple and maintaining the computing cost.

Fig. 15 shows the simulation results for speed control based on the proposed FCS–MPC in the rated speed range of 2000 rpm. The measured speed follows the reference target with good tracking performance at all speeds.

Fig. 16 shows the simulated waveforms in speed control with parameter setting variation. For comparison, the performance of a deadbeat speed control (DBSC), another

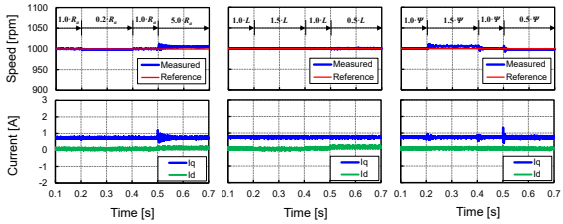

(a) Proposed FCS–MPC with $K_\alpha = 0.9$ and $f_c = 10$ kHz

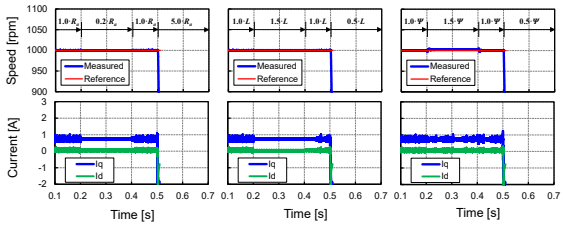

(b) Deadbeat predictive speed control

Fig. 16. Simulation results for speed control under parameter variation (left: resistance; middle: inductance; right: PM flux linkage).

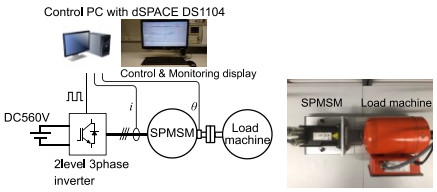

Fig. 17. Test bench constructed for experiments.

predictive control strategy with a modulator, was assessed. More specifically, in the deadbeat-based method, the desired voltage to reach the target speed at the next time step is obtained by a model inverse solution based on (5) to (8), and the output voltage is produced using a PWM modulator. As shown in the results, in the proposed strategy, the parameter mismatch has a small effect on the speed tracking performance. Conversely, in DBSC, the parameter error leads to a destabilization in the speed tracking. It can be said that the proposed method has an advantage for its robustness under the parameter mismatch compared to a deadbeat-based strategy.

B. Experimental results

The performance of the proposed method was assessed using a test rig, as shown in Fig. 17. The control software was implemented on a dSPACE DS1104 real-time system with a 250 MHz microprocessor, and the rotor angular position was measured using an encoder. The load torque was produced by a load machine connected to the SPMSM. In addition, the load machine inertia is unknown to the controller.

Fig. 18 shows the experimental results of the speed control using the FCS–MPC with a voltage smoother. Parameters f_c and K_α were set as the same as those in the simulation presented in Fig. 9. Similarly, the current ripples in the d- and q-axes reduced effectively as K_α increased. In addition, the phase current spectrums under load torque application are presented in Fig. 19.

Figs. 20 and 21 show the performance comparisons between the conventional and proposed FCS–MPC. The parameter settings and load torque corresponded with those from the simulation results presented in Figs. 10 and 12, respectively. Compared with the conventional approach, the current ripples from the proposed method were less. Moreover, as shown in

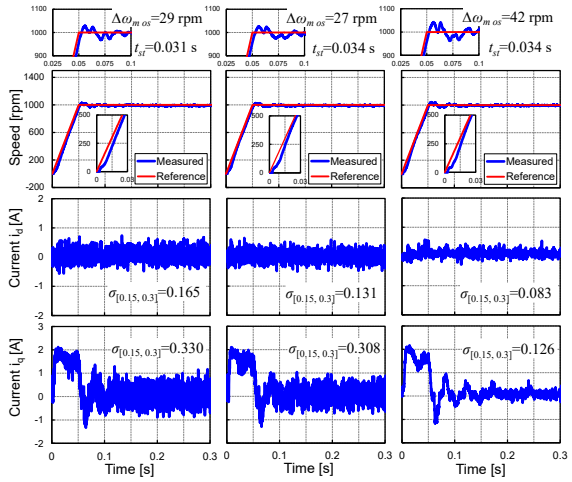

Fig. 18. Experimental results for speed-control-based proposed FCS–MPC with f_c = 10 kHz (left: K_α = 0.3; middle: K_α = 0.6; right: K_α = 0.9).

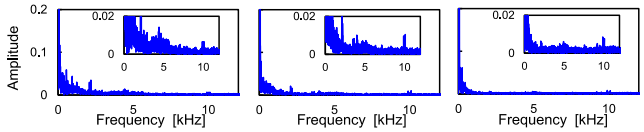

Fig. 19. Frequency spectra of one phase current for the proposed FCS–MPC with f_c = 10 kHz under load torque (left: K_α = 0.3; middle: K_α = 0.6; right: K_α = 0.9).

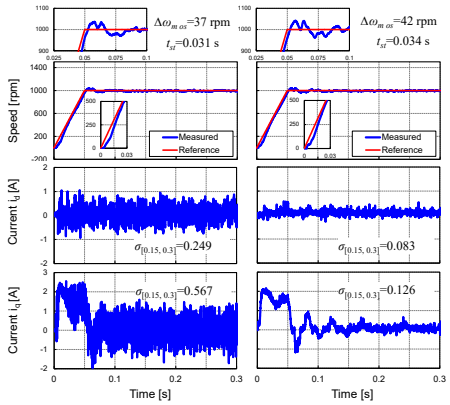

Fig. 20. Experimental results for speed control: comparison with conventional FCS–MPC (left: conventional FCS–MPC; right: proposed FCS–MPC with K_α = 0.9 and f_c = 10 kHz).

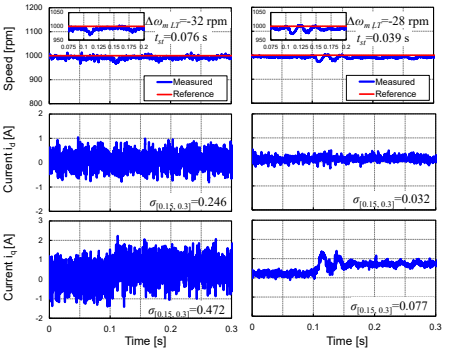

Fig. 21. Experimental results for speed control: comparison with conventional FCS–MPC under load torque change (left: conventional FCS–MPC; right: proposed FCS–MPC with K_α = 0.9 and f_c = 10 kHz).

Fig. 20, the overshoot and settling time were increased compared to those of the conventional method, although not significantly. In Fig. 21, the transient error and settling time of the conventional FCS–MPC were increased compared to those of the proposed method. However, as in the simulation shown in Fig. 12, these increases were caused by the original speed ripple as well as the load torque.

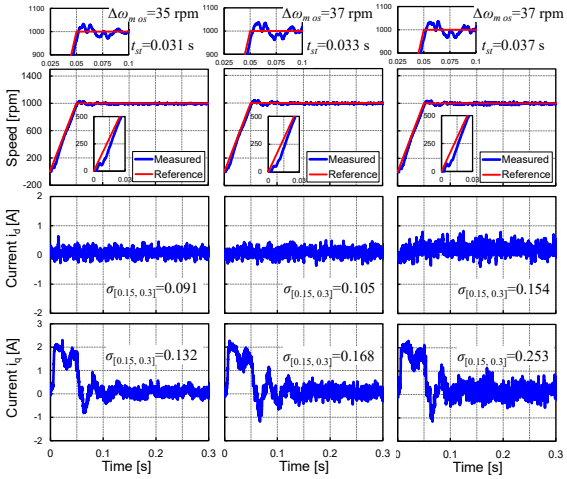

Fig. 22. Experimental results for speed-control-based proposed FCS–MPC with K_α = 0.9 (left: f_c = 8 kHz; middle: f_c = 6 kHz; right: f_c = 3.5 kHz).

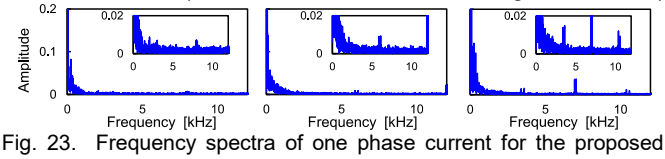

Fig. 23. Frequency spectra of one phase current for the proposed FCS–MPC with K_α = 0.9 under load torque (left: f_c = 8 kHz; middle: f_c = 6 kHz; right: f_c = 3.5 kHz).

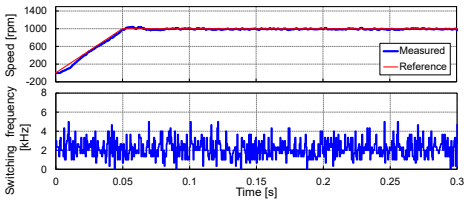

Fig. 24. Experimental result for switching frequency during speed control using conventional FCS–MPC.

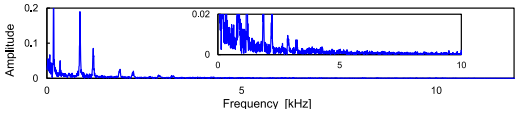

Fig. 25. Frequency spectra of one phase current for the conventional FCS-MPC under load torque.

Fig. 22 shows the experimental results of the carrier frequency variations obtained using the proposed method. In addition, the phase current spectrums are presented in Fig. 23. Although the current ripples in the d- and q-axes increased as the carrier frequency decreased because of the low number of switching, they remained within the permissible range even when the carrier frequency decreased to a level slightly higher than that of the conventional method presented in Fig. 24. It can be said that the proposed method maintains its performance in current ripple suppression while decreasing the switching frequency to the same level as the conventional FCS–MPC. In addition, as shown in the phase current spectrum depict in Fig. 25, differences can be seen in the relatively low frequency components compared to the proposed strategy.

V. Conclusion

In this study, direct speed control based on FCS–MPC with a voltage smoother was presented and applied to a PMSM drive system. The main idea of the proposed strategy is to smooth voltage vector candidates for future current and speed

predictions, as well as to output the optimal smoothed voltage determined using the FCS–MPC scheme.

The simulations and experiments showed that compared with the traditional approach, the proposed method demonstrated favorable servo performance during acceleration as well as in the presence of a load torque change while reducing the current ripples. In addition, the switching frequency can be adjusted by setting the carrier frequency of the pulse-width modulator and reducing it to a slightly higher level than that of the conventional method. To implement the proposed strategy, high additional computational costs are not incurred, and the concept can be implemented on general microprocessors and DSPs other than high-performance processors, such as FPGAs. Owing to its flexibility and simplicity, the proposed concept can be extended to other control types for electric machines, such as current control and angular position control, as well as to other power electronics applications.

REFERENCES

[1] R. Gabriel, W. Leonhard, and C. Nordby, “Field-Oriented Control of a Standard AC Motor Using Microprocessors,” IEEE Trans. Ind. Appl., vol. IA–16, no. 2, pp. 186–192, Mar. 1980.

[2] K.S. Rajashekara and J. Vithayathil, “Current Impressed Voltage Source Inverter Fed Induction Motor Control by Field Orientation,” Can. Elec. Eng. J., Vol.8, no. 4, pp. 135–141, 1983.

[3] B.K. Bose and P.M. Szczesny, “A Micro-computer-Based Control and Simulation of an Advanced IPM Synchronous Machine Drive Syst em for Electric Vehicle Propulsion,” IEEE Trans. Ind. Electron., vol.35, no.4, pp.547–559, Nov. 1988.

[4] P. Cortés, M. Kazmierkowski, R. Kennel, D. Quevedo, and J. Rodríguez., “Predictive Control in Power Electronics and Drives,” IEEE Trans. Ind. Electron., vol. 55, no. 12, pp. 4312–4324, Dec. 2008.

[5] S. Vazquez, J.I. Leon, L.G. Franquelo, J. Rodriguez, H.A. Young, A. Marquez and P. Zanchetta, "Model Predictive Control: A Review of Its Appli cations in Power Electronics," in IEEE Industrial Electronics Magazine, vol. 8, no. 1, pp. 16-31, Mar. 2014.

[6] R. Kennel, A. Linder and M. Linke, "Generalized predictive control (GPC)-ready for use in drive applications?," 2001 IEEE 32nd Annual Power Electronics Specialists Conference, Vancouver, BC, 2001, pp. 1839-1844 vol. 4.

[7] A. Linder and R. Kennel, "Model Predictive Control for Electrical Drives," 2005 IEEE 36th Power Electronics Specialists Conference, Recife, 2005, pp. 1793-1799.

[8] S. Mariethoz and M. Morari, “Explicit model-predictive control of a pwm inverter with an lcl filter,” IEEE Trans. Ind. Electron., vol. 56, no. 2, pp. 389–399, Feb. 2009.

[9] J. Rodríguez, J. Pontt, P. Correa, P. Lezana and P. Cortés, “Predictive power control of an AC/DC/AC converter,” in Proc. IEEE 40th Annual Meeting Industry Appl. Society, Hong Kong, Oct. 2005, pp.934–939.

[10] J. Rodríguez, J. Pontt, C. Silva, P. Correa, P. Lezana, P. Cortés, and U. Ammann, “Predictive current control of a voltage source inverter,” IEEE Trans. Ind. Electron., vol. 54, no. 1, pp. 495–503, Feb. 2007.

[11] J. Rodriguez, M. Kazmierkowski, J. Espinoza, P. Zanchetta, H. Abu-Rub, H. Young, C. Rojas "State of the Art of Finite Control Set Model Predictive Control in Power Electronics," in IEEE Transactions on Industrial Informatics, vol. 9, no. 2, pp. 1003-1016, May 2013

[12] T. Geyer and D. E. Quevedo, "Multistep Finite Control Set Model Predictive Control for Power Electronics," in IEEE Transactions on Power Electronics, vol. 29, no. 12, pp. 6836-6846, Dec. 2014.

[13] S. A. Davari, D. A. Khaburi and R. Kennel, “An improved FCS-MPC algorithm for an induction motor with an imposed optimized weighting factor,” IEEE Trans. Power Electron., vol. 27, no. 3, pp. 1540–1551, Mar. 2012.

[14] C.A. Rojas, J. Rodriguez, F. Villarroel, J.R. Espinoza, C.A. Silva, M. Trincado, “Predictive Torque and Flux Control Without Weighting Factors”, IEEE Trans. Ind. Electron., vol. 60, no. 2, pp. 681–690, Feb. 2013.

[15] F. Wang, Z. Zhang, S. A D, R. Fotouhi, D A. Khaburi, J. Rodríguez and R. Kennel, “An Encoderless Predictive Torque Control for an Induction Machine With a Revised Prediction Model and EFOSMO”, IEEE Trans. Ind. Electron., vol. 61, no. 12, Dec. 2014.

[16] A. Linder and R. Kennel, “Direct model predictive control—A new direct predictive control strategy for electrical drives,” in Proc. Eur. Conf. Power Electron. Appl., Sep. 2005.

[17] S. Chai and L. Wang; "Finite Control Set Model Predictive Control of 2LVSI-PMSM using interpolated switching states, "IECON 2012 the 38th Annual Conference on IEEE Industrial Electronics Society, pp.1799-1804, Oct. 2012.

[18] A. Formentini, A. Trentin, M. Marchesoni, P. Zanchetta and P. Wheeler, "Speed Finite Control Set Model Predictive Control of a PMSM Fed by Matrix Converter," IEEE Trans. Ind. Electron., vol. 62, no. 11, pp. 6786-6796, Nov. 2015.

[19] Y. Hozumi, S. Doki and S. Okuma, “Fast Torque Control System of PMSM based on Model Predictive Control”, IECON 2009 the 35th Annual Conference on IEEE Industrial Electronics Society, pp.1147-1151, Oct. 2009.

[20] T. Zanma, M. Kawasaki, K.Z. Liu, M. Hagino and A. Imura, “Model Predictive Direct Torque Control for PMSM with Discrete Voltage Vectors”, IEEJ Trans Elec Electron Eng, pp. 121-130, vol.3, no.2, 2014.

[21] M. Preindl and S. Bolognani, “Model predictive direct speed control with finite control set of PMSM-VSI drive systems,” in Workshop on Predictive Control of Electrical Drives and Power Electronics (PRECEDE), Munich, Germany, pp. 17–23, Oct. 2011.

[22] M. Preindl and S. Bolognani, “Model predictive direct speed control with finite control set of PMSM drive systems,” IEEE Trans. Power Electron., vol. 28, no. 2, pp. 1007–1015, Feb. 2013.

[23] E. Fuentes, D. Kalise, J. Rodriguez, and R. Kennel, “Cascade-Free Predictive Speed Control for Electrical Drives,” IEEE Trans. Ind. Electron., vol. 61, no. 5, pp. 2176–2184, May 2014.

[24] H. Kawai, Z. Zhang and R. Kennel, “Finite Control Set-Model Predictive Speed Control with a Voltage Smoother”, IECON 2018 the 44th Annual Conference on IEEE Industrial Electronics Society, pp.528-533, Oct. 2018.

[25] P. Stolze, P. Karamanakos, R. Kennel, S. Manias, and T. Mouton, “Variable switching point predictive torque control for the three-level neutral point clamped inverter,” in Proc. Eur. Power Electron. Conf., Lille, France, Sep. 2013.

[26] P. Karamanakos, P. Stolze, R. M. Kennel, S. Manias and H. T. Mouton, "Variable Switching Point Predictive Torque Control of Induction Machines," in IEEE Journal of Emerging and Selected Topics in Power Electronics, vol. 2, no. 2, pp. 285-295, June 2014.

[27] W. Il-Kuen; H. Jun-Ha; K. Do-Yun; J. Young-Hee; W. Chung-Yuen, “Performance improvement of IPMSM using finite predictive current control for EV,” in Future Energy Electronics Conference (IFEEC), 2015 IEEE 2nd International, pp.1–7, Nov. 2015.

[28] M. Shimaoka and S. Doki, “Design of search space for improving the steady current control performance of PMSM current control system based on model predictive control”, IEEJ Trans Ind. Application, Vol.140, no. 6, pp. 468–479, 2020.

[29] S.-M. Yang and C.-H. Lee, “A deadbeat current controller for field oriented induction motor drives,” IEEE Trans. Power Electron., vol. 17, no. 5, pp. 772–778, Sep. 2002.

[30] X. Zhang, B. Hou, and Y. Mei, "Deadbeat predictive current control of permanent-magnet synchronous motors with stator current and disturbance observer", IEEE Trans. Power Electron., vol. 32, no. 5, pp. 3818–3834, May 2017.

[31] L. Verkroost, J. Druant, H. Vansompel, F. De Belie and P. Sergeant, "Predictive Current Control vs. PI Control for Surface Mounted Permanent Magnet Machines," 2018 XIII International Conference on Electrical Machines (ICEM), pp. 1663-1669, Oct. 2018.

[32] Z. Zedong, L. Yongdong, M. Fadel, and X. Xi, “A rotor speed and load torque observer for pmsm based on extended kalman filter,” in 2006, IEEE International Conference on Industrial Technology, pp. 233–238, Dec 2006.

[33] M. Iwasaki and N. Matsui, “High Performance Speed Control System

of Vector Controlled Induction Motor with Load Torque Observer," IEEJ Trans Elec Electron Eng, Vol. 110–D, no. 11, pp.1126–1132, 1990.

[34] H. Kawai, Z. Zhang and R. Kennel, "Finite Control Set Model Predictive Speed Control with a Load Torque Compensation," IEEJ Trans Elec Electron Eng, Vol. 15, no.10, pp. 1530-1540, 2020.

[35] P. Cortes, J. Rodriguez, C. Silva, A. Flores, "Delay compensation in model predictive current control of a three-phase inverter.", IEEE Trans. Ind. Electron., vol. 59, no. 2, pp. 1323–1325, Feb. 2012.

Hiroaki Kawai (M'18) was born in Hyogo, Japan, in 1983. He received the B.E. and M.E. degrees in mechanical system engineering from Hiroshima University, Japan, in 2005 and 2007, respectively. Since 2007, he has been with Kobe Steel, Ltd., Japan, where he is currently a Senior Researcher in the Technical Development Group. From 2016 to 2017, he was a Guest Researcher at the Institute for Electrical Drive Systems and Power Electronics, Technical University of Munich, Munich, Germany. He is currently working toward the Ph.D. degree at Nagoya University, Japan. His research interests include system control, predictive control, power electronics and electrical drives.

Zhenbin Zhang (S'13–M'16–SM'18) was born in Shandong, China, in 1984. He received the Ph.D. degree at the Institute for Electrical Drive Systems and Power Electronics (EAL), Technical University of Munich (TUM), Germany, with "summa cum laude". From 2016 to 2017, he worked as a Research Fellow and the group-leader for "Modern control strategies for electrical drives" group in EAL of TUM. Since 2017, he has been a full professor and lab.-director at Shandong Uni., Jinan, China. Since 2020, he has been appointed as the director of International Center for Intelligent Energy and Power Conversion Systems (IEPCS) at Shandong Uni. Dr. Zhang received the VDE-Award, Sued bayern, Germany, in 2017. His research interests include power electronics and electrical drives, sustainable energy systems, smart- and micro-grid.

Ralph Kennel (M'89-SM'96) was born in 1955 at Kaiserslautern (Germany). In 1979 he got his diploma degree and in 1984 his Dr.-Ing. (Ph.D) degree from the University of Kaiserslautem. From 1983 to 1999 he held on several positions with Robert Bosch GmbH (Germany). Until 1997 he was responsible for the development of servo drives. From 1994 to 1999 Dr. Kennel was appointed Visiting Professor at the University of Newcastle-upon-Tyne (England, UK). From 1999 to 2008 he was Professor for Electrical Machines and Drives at Wuppertal University (Germany). Since 2008 he has been Professor for Electrical Drive Systems and Power Electronics at the Technical University of Munich (Germany). His main interests today are: Sensorless control of AC drives, predictive control of power electronics and Hardware-in-the-loop systems. Dr. Kennel is a Senior Member of IEEE, a Fellow of IET and a Chartered Engineer in the UK. Within IEEE he is Treasurer of the Germany Section as well as ECCE Global Partnership Chair of the Power Electronics society (PELS).

Shinji Doki was born in Nagoya, Japan in 1966. He received the BE, ME and PhD degrees in Electronic-mechanical Engineering from Nagoya University, Japan in 1990, 1992 and 1995, respectively. Since 2012, He has been a Professor at Nagoya University, Japan. His research interests are in the area of control, modeling, signal / information processing and its application for motor drive system. Dr. Doki received the IEEE IECON'92 best paper award, the paper awards from FANUC FA and Robot Foundation, the Institute of Electrical Engineers of Japan(2004, 20015) and Best Paper Award of the 20th IEEE International Conference on Electrical Machines and Systems 2017 .